Ultrasonically Enhanced Desalting of Cod (*Gadus morhua*). Mass Transport Kinetics and Structural Changes

César Ozuna [a], Ana Puig [b], Jose V. Garcia-Perez [a], and Juan A. Cárcel[a,*]

[a] Grupo de Análisis y Simulación de Procesos Agroalimentarios. Departamento de Tecnología de Alimentos. Universitat Politècnica de València.

Camino de Vera. s/n. E46022. Valencia, Spain

[b] Grupo de Microestructura y Química de Alimentos. Departamento de Tecnología de Alimentos. Universitat Politècnica de València.

Camino de Vera. s/n. E46022. Valencia, Spain

*Corresponding author.

Juan A. Cárcel.

Grupo de Análisis y Simulación de Procesos Agroalimentarios. Departamento de Tecnología de Alimentos. Universitat Politècnica de València.

Camino de Vera. s/n. E46022. Valencia, Spain

Tel.: +34 96 387 93 65; Fax: +34 96 387 98 39

E-mail address: jcarcel@tal.upv.es.

ABSTRACT

The search for an alternative means of reconstituting dried and salted products prior to consumption is of relevance for the food industry. New techniques should speed up the process while causing minimum impact on product quality. Thereby, the aim of this work was to evaluate both the effect of high-intensity ultrasound application on the desalting kinetics of cod, as well as the changes in its textural and microstructural properties. Moisture and NaCl transport was studied separately by taking the diffusion theory into account. The evolution in the swelling and hardness of cod during desalting was determined and modeled by assuming first-order kinetics. A microstructural analysis of raw salted and desalted cod was also carried out by means of light microscopy and SEM techniques. Ultrasound application significantly ($p<0.05$) affected both moisture and NaCl transport and the increase in both effective diffusivities (from 24% to 103%) was linked to the acoustic pressure applied. The desalting process induced the swelling and the softening of the cod tissue, both of which are phenomena that are intensified by ultrasound application. From the microstructural observations, it was shown that the application of high-intensity ultrasound modified the cod structure, e.g. the increase in the fiber width.

Keywords: Ultrasound, Modeling, Diffusivity, Texture, Microscopy.

1. Introduction

Salted cod (*Gadus morhua*) is one of the most widely-consumed heavy-salted products in southern European countries and Latin America (Martínez-Alvarez & Gómez-Guillén, 2013; Oliveira, Pedro, Nunes, Costa, & Vaz-Pires, 2012). Due to the unpalatably high salt concentration in the fish muscle, cod must be desalted before consumption. This process is traditionally carried out by immersing the product in stagnant water over a period of 24–48 h. Thus, desalting is accomplished not only through the loss of salt but also as a result of sample rehydration (Barat, Rodríguez-Barona, Andrés & Visquert, 2004). The combined effect of water gain and salt loss on the protein matrix (Thorarinsdottir et al., 2011) modifies the structure of product. Protein rehydration involves a loss of firmness (Barat et al., 2004). Moreover, the reduction in NaCl content improves the water holding capacity, which, in turn, increases the water absorption, thus contributing to the total weight gain (Oliveira et al., 2012).

The main problems of industry-scale cod desalting are linked to the final product quality and long processing times. For this reason, recent research has focused on finding new cod desalting methods in order to improve the mass transfer process, like tumbling technology (Bjørkevoll, Olsen, & Olsen, 2004), vacuum pulses (Andrés, Rodríguez-Barona, and Barat, 2005) or high pressures (Salvador, Saraiva, Fidalgo and Delgadillo, 2013).

High-intensity ultrasound (**US**) is being used as a novel food process intensification technique (Chemat, Zill-e-Huma, & Khan, 2011; Pananun, Montalbo-Lomboy, Noomhorm, Grewell, & Lamsal, 2012). In liquid media, US enhances mass transfer mainly by inducing cavitation (Ozuna, Puig, García-Pérez, Mulet, & Cárcel, 2013). In addition, some other mechanical phenomena, such as the “sponge effect” (Cárcel, Benedito, Rosselló, & Mulet, 2007a), the generation of microchannels in the solid or microstirring at the solid-liquid interfaces, could also affect both the external and internal mass transfer resistance (Fernandes, Gallão, & Rodrigues, 2008). Moreover, the mechanical stress that US causes in the product may modify both structural and textural properties (Gabaldón-Leyva et al., 2007; Stadnik, Dolatowski, & Baranowska, 2008). The effectiveness of applying US is directly linked to the actual acoustic energy introduced in the medium (Kulkarni & Rathod, 2014). This fact mainly depends on the emitter-liquid-product coupling, which should be experimentally determined in each specific application (Cárcel, Benedito, Bon, & Mulet, 2007b).

US has been used to enhance mass transport in the treatments of solids in hypertonic solutions, such as meat or cheese brining (Ozuna et al., 2013; Siró et al., 2009; Cárcel et al., 2007b; Sanchez et al., 1999). However, as far as we are concerned, there is no previous literature on the use of US to improve the desalting of foodstuffs. Therefore, the aim of this work was to evaluate the feasibility of using US in cod desalting from the study of the mass transport kinetics, texture evolution and microstructure of desalted samples.

2. Materials and Methods

2.1 Raw material and sample preparation

Salted cod (*Gadus morhua*) pieces (1.50±0.25 kg) were provided by a local supplier (Carmen Cambra S. L., Spain) to ensure the homogeneity of the raw material. Parallelepiped-shaped samples (length 50 x width 30 x thickness 5 mm) were obtained from the central part of the cod loin using a sharp knife, wrapped in plastic waterproof film and kept refrigerated at 2±0.5 ºC (maximum storage time 120 h) until the desalting experiments.

2.2 Ultrasonic equipment

The desalting treatments were carried out in an ultrasonic bath (71 L, 40 kHz; ATU Ultrasonidos, Spain), equipped with a cooling jacket (Fig. 1F). The equipment allows the applied ultrasonic power to be modulated (up to 1500 W) (Fig. 1L). For the temperature control, a glycol solution was pumped (1-38023 CLES, EBARA, Italy) (Fig. 1D) from a reservoir tank (Fig. 1E) into the cooling jacket. Afterwards, the glycol solution was cooled down in a plate heat exchanger connected to a chiller unit (Fig. 1A). The temperature in the bath was measured using seven type K thermocouples (Fig. 1H), placed in different positions and connected to a data logger (HP Data Logger 34970 A, Hewlett-Packard S.A., Spain) (Fig. 1K).

2.3 Characterization of the acoustic field

Two different techniques were used to estimate the actual ultrasonic energy applied: calorimetry and acoustic pressure determination. The measurements were carried out at a depth of 100 mm from the water-air interface, where samples were placed during treatment. This depth corresponded to a maximum pressure plane detected through the erosion planes produced by cavitation on a piece of aluminum foil.

The calorimetric method consisted of recording the temperature at 7 different points (Fig. 1H) for the first 1 min of US application (Cárcel et al., 2007b). At least five replicates were carried out for each measurement. The slope of the temperature vs. time curve gave an estimation of the average ultrasonic power in the medium.

The acoustic pressure measurement was carried out with a hydrophone (TC4013, Reson A/S, Denmark) connected to a digital oscilloscope (Tektronix TDS 420 A, Tektronix Inc., USA). The output voltage level (average of 100 signal acquisitions) was converted into the equivalent acoustic pressure (bar) by using the known sensitivity of the hydrophone. For the measurement, 2D scans were performed by moving the hydrophone in 30 mm increments in both X and Y-directions. In such a way, the surface of the ultrasonic bath (length 600 and width 300 mm) was mapped by measuring the acoustic pressure in a rectangular mesh of 171 nodes.

2.4 Desalting experiments

Before each desalting experiment, samples were immersed in distilled water for 20 s to remove the superficially adhered salt. Then samples were blotted and weighed (PB3002-S/PH, J.P., Mettler Toledo, Spain). Afterwards, 28 samples were placed in a sample holder (Fig. 1G) and introduced into the ultrasonic bath containing 27 L of low-mineral content water (Cortes, S.A., Spain). Three sets of desalting experiments were carried out: without (CONTROL) and with US application at two different electric powers: 1500 W (US-1500) and 750 W (US-750). At least 3 replicates were made for each treatment tested.

At preset times (15, 30, 45, 60, 90, 120 and 180 minutes), four samples were randomly taken out of the bath, blotted, wrapped in plastic waterproof film and frozen (-18 ± 0.5 ºC) until moisture (method No. 950.46 AOAC, 1997) and NaCl content (Cárcel et al., 2007b) were determined; this was carried out in triplicate in each case.

The thickness of each sample was measured before (T_0) and after (T) desalting with a Vernier caliper and the thickness ratio (TR) (Eq. 1) was estimated as an index of swelling.

$$TR = \frac{T}{T_0} \qquad (1)$$

Hardness (H), characterized as the maximum penetration force, was also evaluated in desalted cod samples at different times using a Texture Analyzer (TAX-T2®, Stable

Micro System, United Kingdom). Penetration tests were conducted with a 2 mm flat cylinder probe (SMS P/2N), at a crosshead speed of 1 mm/s and a strain of 70% (penetration distance 3.5 mm). In each cod sample, a preset pattern was followed in order to carry out penetration tests at, at least, 12 different points.

2.5 Mathematical modeling

2.5.1 Moisture and NaCl transport

A simple mathematical model based on Fick's 2nd law (Crank, 1975) was used as a first approach (Carcel et al., 2007a; Garau, Simal, Femenia &, Rosselló, 2006) to describe the evolution of moisture and NaCl content in the samples during desalting. Mass transport was considered to be one-dimensional due to the fact that thickness (5 mm) was 1/6 (30 mm) and 1/10 (50 mm) shorter than the other dimensions. The mass flow in the thickness direction being much larger compared to the other ones due to the relative mass transfer resistances (Singh & Heldman, 2001). Thus, approaching the slices as infinite slabs sounds reasonable (Garau et al. 2006). Constant effective diffusivities (D_{NaCl} and D_W), negligible changes in temperature and sample volume, solid symmetry, homogeneous initial NaCl and moisture contents and negligible external resistance were assumed. Eqs. 2 and 3 show the solution of the diffusion model in terms of the average moisture and NaCl content, respectively (Ozuna et al., 2013).

$$W = W_{eq} + (W_0 - W_{eq})\left[2\sum_{n=0}^{\infty}\frac{1}{\lambda_n^2 L^2}e^{-D_W \lambda_n^2 t}\right] \quad (2)$$

$$NaCl = NaCl_{eq} + \left(NaCl_0 - NaCl_{eq}\right)\left[2\sum_{n=0}^{\infty}\frac{1}{\lambda_n^2 L^2}e^{-D_{NaCl} \lambda_n^2 t}\right] \quad (3)$$

where, λ_n are the eigenvalues that are calculated by $\lambda_n L = (2n+1)\frac{\pi}{2}$. In these conditions and from a theoretical point of view, the effective diffusivity was considered to be the only kinetic parameter that involved all the effects which influenced the moisture or NaCl transport rate. However, in practice the effective diffusivity identified by fitting the model to the experimental data included all unknown mechanisms that affected the mass transfer kinetics (external resistance, sample swelling, etc.).

2.5.2 Evolution of hardness and swelling

First-order reaction models, widely used to describe the kinetics of structural changes in processed foods (Blasco, Esteve, Frígola, & Rodrigo, 2004; Baik & Mittal, 2003), were considered to study the evolution of the thickness ratio (Eq. 4) and hardness (Eq. 5) during desalting.

$$TR = TR_{eq} + (TR_0 - TR_{eq})e^{(-k_{TR} \cdot t)} \quad (4)$$

$$H = H_{eq} + (H_0 - H_{eq})e^{(-k_H \cdot t)} \quad (5)$$

2.6 Model fitting

The parametric identification of the first order kinetics (k_{TR}, TR_{eq}, k_H and H_{eq}) and the diffusion models (D_{NaCl}, D_W) was carried out by using an optimization procedure (Generalized Reduced Gradient) that minimized the sum of the squared differences between the experimental and calculated data. The goodness of the fit was determined by assessing the percentage of explained variance, VAR (%) (Eq. 6).

$$VAR(\%) = \left[1 - \frac{S_{xy}^2}{S_y^2}\right] \cdot 100 \quad (6)$$

2.7 Microstructure

2.7.1 Scanning electron microscopy with combined dispersion X-ray analysis (SEM-EDX).

Cubic samples (side 3 mm) of salted and desalted cod (CONTROL, US-750 and US-1500 after 180 min of desalting) were immersed in liquid nitrogen and then freeze-dried at 1 Pa for 3 days (LIOALFA-6, Telstar, Spain). Then the samples were vacuum sealed in vials in the same freeze-drier so that they would remain stable (Hernando, Llorca, Puig, & Lluch, 2011). After that, they were individually placed on SEM slides with the aid of colloidal silver and then gold-coated with carbon (SCD005, Baltec, Germany) at 10^{-2} Pa and an ionization current of 40 mA. The samples were observed through a scanning electron microscope (JSM-5410, Jeol, Japan) equipped with an X-ray detector and LINK data-processing system (INCA 4.09, Oxford Instruments, England) at an acceleration voltage of 10-20 kV, which provides internal information about the standards of the energy dispersive X-ray spectra of the elements analyzed, Na^+ and Cl^- (Ozuna et al., 2013). For the EDX (energy-dispersive X-ray) analysis, the samples were carbon-coated (CEA035, Baltec, Germany). Mapping images of the Cl^- and Na^+ distribution in cod samples were taken using a voltage of 20 kV and at a working distance of 15 mm.

2.7.2 Light microscopy (LM)

For LM observation, cryostat sections (200 µm) were obtained from frozen desalted cod (CONTROL, US-750 and US-1500 after 180 min of desalting) using a CM1950 microtome (Leica Biosystems, Germany). The sections were transferred to coated glass slides, which had previously been placed inside the cryo chamber to achieve an improved adherence of the tissue sections (Thorarinsdottir et al., 2011). The cryostat section samples were examined under a light microscope (Nikon Eclipse E800, Japan).

The fiber thickness was measured from micrographs obtained by both light microscopy and SEM-EDX using the ImageJ 1.44d software (Wayne Rasband, National Institute of Health, USA). All the measurements were assessed from at least six randomly acquired images.

3. Results and Discussion

3.1 Acoustic field characterization

The acoustic field characterization was carried out at the two different levels of electric power used in the ultrasonically assisted desalting experiments: 750 W (US-750) and 1500 W (US-1500).

From the calorimetric measurements, it could be observed that the average volumetric energy available in the medium was 19±5 kW/m^3 and 37.9±5.2 kW/m^3 for US-750 and US-1500, respectively. The calorimetric/electric yields were close to 70%.

The acoustic pressure measurements showed a very irregular acoustic field distribution in the bath (Figs. 2A and 2B): the acoustic field pattern for US-750 was different from that for US-1500. The reflections of ultrasonic waves at the moving air-water interface or the bath walls and the implosions of cavitation bubbles (Kulkarni & Rathod, 2014) can generate this heterogeneous ultrasonic field. As regards the integrated average acoustic pressure, it was 0.5±0.1 bar (Fig. 2B; range 0.3-0.8 bar) for US-1500, but 0.4±0.1 bar (Fig. 2A; range 0.1-0.7 bar) for US-750.

As can be observed, doubling the electric energy supplied to the bath transducers doubles the energy measured by calorimetry but not that measured using the hydrophone.

The calorimetric method measured the thermal effects produced by US, while acoustic pressure is a measurement of only mechanical effects. The interaction between waves produced by reflections or cavitation can partially neutralize them producing a conversion of acoustic energy into heat. Therefore, acoustic pressure is a more accurate measurement of the ultrasonic mechanical energy available to produce effects.

3.2 Mass transport

3.2.1 Experimental NaCl and water content

Salted cod loin showed an initial NaCl content of 0.6±0.2 kg NaCl/kg SFS (salt-free solids). The immersion of samples in water produced a decrease in NaCl content, which was greater when US was applied (Fig. 3A). Thus, after 180 min of desalting, the NaCl content in US-1500 (0.114±0.007 kg NaCl/kg SFS) was 32% lower than that measured in CONTROL samples (0.17±0.03 kg NaCl/kg SFS). US-750 showed an intermediate NaCl content (0.13±0.04 kg NaCl/kg SFS). Therefore, the influence of US depended on the acoustic power applied (Fig. 3A).

As regards the moisture content, the cod loin's initial content of 1.9±0.2 kg water/kg SFS increased during the experiments. The US application also significantly ($p<0.05$) accelerated the water transport (Fig. 3B). For example, the moisture content of CONTROL after 180 min of treatment (3.0±0.4 kg water/kg SFS) was achieved for US-1500 in only 63 min (65% reduction in treatment time). As in the case of NaCl transport, the water gain was dependent on the acoustic power applied.

3.2.2 Modeling transport kinetics

The fit of the proposed diffusion models to the experimental data provided percentages of explained variance ranging from 93 to 95% for NaCl and 95 to 97% for moisture kinetics (Table 1). These low values can be attributed to the great variability of the raw material (Oliveira et al., 2012; Barat et al., 2004). However, the trend between calculated and experimental data was quite similar (Fig. 3), showing the feasibility of the model.

The D_{NaCl} values identified for CONTROL (4.57 x 10^{-10} m^2/s) were in the same order of magnitude as others found in literature (Barat et al., 2006 and 2004) for cod desalting. The application of US during desalting produced a significant ($p<0.05$) increase in D_{NaCl}, which depended on the power applied. Thus, D_{NaCl} was 25% higher for US-750 and 62% higher for US-1500 than the figure identified for CONTROL experiments (Table 1). The relationship between the applied acoustic energy and the identified D_{NaCl} was better described from acoustic pressure measurements than from calorimetric. Between the US-750 and US-1500 experiments there was observed to be a 30% increase in acoustic pressure (from 0.39 bar to 0.51 bar, respectively) and this provided a close fit to the 30% increase in the identified D_{NaCl} (Table 1), while using calorimetry, an effective diffusivity increase of 103% would be expected. During the desalting experiments, the temperature was held at 4 ºC and, as a result, only ultrasonic mechanical effects on mass transport took place, which are well quantified from the acoustic pressure measurement. Calorimetric measurements, on the other hand, are more suitable for quantifying the thermal effects produced by ultrasound.

In the case of moisture transport, the increase in D_W brought about by US application was close to 41% for US-750 and 103% for US-1500 as compared to CONTROL experiments. As in the case of D_{NaCl}, the increase in D_W was also well correlated with the increase in acoustic pressure.

The increase in solute and moisture transport when applying ultrasound has been previously described in other solid-liquid systems. Thus, Siró et al. (2009) found increases of 96% in D_{NaCl} when US was applied during meat brining (5 ºC, 4% NaCl), and Gabaldón-Leyva et al. (2007) observed an improvement of 190% in the total solid diffusion coefficients during the brining of bell pepper (55 ºC, 13.51% NaCl). Ozuna et al. (2013) reported increases in D_W of around 101% when US was applied in meat brining (5 ºC, 28% NaCl) and Cárcel et al. (2007a) found increases of 117% in moisture transport during the osmotic dehydration of apple (30 ºC, 30 ºBrix).

It should be pointed out that, even the proposed theoretical model considers the moisture and NaCl transport only controlled by diffusion, the effective diffusivities (D_{NaCl} and D_W) identified are just kinetic parameters, which also include other phenomena affecting the mass transport, such as external convective flow or volume sample changes (Mulet, 1994) like swelling. The influence of US on mass transport comes from the appearance of effects such as the so-called "sponge effect" or the generation of microchannels (Cárcel et al., 2010) that reduce the internal resistance and the generation of microstirring or the implosion of cavitation bubbles at interfaces that enhance the external mass transport (Chemat et al., 2011). As previously explained, temperature control avoids any improvement linked to thermal energy.

3.3 Evolution of swelling

The application of US during desalting increased the swelling, measured from the TR (Eq. 1), and this increase depended on the level of acoustic power applied (Fig. 4A). Thus, after 180 min desalting, while US-750 samples showed a TR value (2.8±0.1) which was 22% higher than that of CONTROL (2.3±0.4), in the case of US-1500 there was a 50% increase (3.4±0.3).

As for the experimental variability, the first order kinetic (Eq. 4) provided an adequate estimation of the TR (Table 2). The rate constant (k_{TR}), which is related with the rate of swelling during desalting, was not significantly ($p<0.05$) increased by US application

(Table 2). As can be observed in Fig. 4B, there was no direct kinetic effect on the swelling itself produced by US, but the influence observed on the experimentally measured swelling can be simply linked to the fact that US application intensified water transport.

3.4 Evolution of hardness

The measurements of the maximum penetration force showed that the initial degree of hardness of the salted cod (3.6±0.4 N) reduced as the desalting process progressed (Fig. 5). Major hardness changes took place in the first 45 min and an asymptotic value was found after approximately 60 min of desalting (Fig. 5A). US application accelerated this reduction in hardness (Fig. 5A), with the greatest differences between CONTROL and US experiments observed at the beginning of the desalting. Unlike what was observed in the case of swelling, the influence of US on the evolution of hardness can be attributed not only to the ultrasonic intensification of mass transport but also to some textural effects (Stadnik et al., 2008), since, at a similar water content, US samples exhibited a lower hardness value than CONTROL (Fig. 5B). No differences were observed between US-750 and US-1500.

The ability of US to induce structural effects has already been reported (Gabaldón-Leyva et al. 2007; Ozuna et al., 2013). The compressions and expansions produced by US induced mechanical stress on both the protein structure and the constituents of the connective tissue that can lead to softening.

The first-order kinetic model (Eq. 5) accurately described the hardness changes during desalting (Fig. 5A). Both model parameters (k_H and H_{eq}) were significantly ($p<0.05$) affected by US application. However, no significant differences were found between the two acoustic powers tested (Table 2). The rate constant (K_H) significantly ($p<0.05$)

increased when acoustic energy was applied as indicated by the more marked reduction in hardness when US was applied (Fig. 5B). The equilibrium hardness value (H_{eq}) was lower for US treatments than CONTROL, which may be ascribed to the abovementioned structural effects of US.

3.5 Microstructure

SEM micrographs showed the microstructure of salted cod (Fig. 6). The cod fibers, covered by salt deposits (Fig. 6A), presented an intense dehydration and compaction with a total degradation of connective tissue. The high content of salt masked the underlying structures (Fig. 6B). During desalting, important changes take place as a consequence of cell rehydration. After 180 min of treatment, samples showed a significant swelling of muscle fibers (Figs. 7A, 7B and 7C) compared to salted cod (Fig. 6). Thus, the fibers' average width increased from 64.4±9.2 µm in the case of salted cod fibers to 84.1±11.7 µm in CONTROL samples. This increase was even greater when US was applied (Figs. 7B and 7C). In this sense, US-1500 fibers (Fig. 7C) were 27% wider (106.7±11.5 µm) than CONTROL. This fiber width increase was also observed in LM micrographs. In this case, the measured fiber width increased from 90.4±4.4 µm in CONTROL (Fig. 7D) to 108.8±13.2 and 139.4±11.7 µm in US-750 (Fig. 7E) and US-1500 (Fig. 7F), respectively. The differences between LM and SEM measurements can be attributed to the differences in sample preparation.

The fiber width increase explains the macroscopic swelling already described in Fig. 4. In addition, the US application increased the interfibrillar spaces (IS) (Figs. 7B and 7C) that can also contribute to the softening of US samples (Fig. 5). The SEM-EDX technique confirmed that US application intensified the NaCl leakage (Figs. 7B and

7C), which was manifested by a lower number of dots in micrographs than in CONTROL (Fig. 7A).

The LM micrographs also showed the mechanical effects of acoustic energy. The US samples presented greater fiber and connective tissue degradation (Figs. 7E and 7F) than CONTROL (Fig. 7D). This fact can be attributed to violent microjets produced by the asymmetric implosion of bubbles near the solid surface. These results coincide with those found by other authors who related the application of US with the physical disruption of the myofibril structure (Ozuna et al., 2013), the degradation of collagen macromolecules, or the creation of micro-channels (Jayasooriya, Bhandari, Torley, & D'Arcy, 2004).

4. Conclusions

The application of high-intensity ultrasound improved cod desalting, increasing both moisture and NaCl effective diffusivities by up to 103 and 62%, respectively. The desalting induced the tissue swelling and the decrease in sample hardness, both of which were intensified by ultrasound application. Microstructural analyses showed that cod fibers were significantly affected by ultrasound application. These facts not only coincide with the intensification of mass transport and the observed enhancement of swelling, but also with the decrease in hardness.

Acknowledgments

The authors acknowledge the financial support of the Spanish Ministerio de Economía y Competitividad and FEDER (Ref. DPI2013-37466-C03-03). César Ozuna thanks Universitat Politècnica de València for an FPI grant (Ref. 2009-02). The author also wishes to thank Carmen Cambra S.L. for selecting the raw material.

Nomenclature

Symbol	Reference	Unit
SFS	Salt-free solids	
W_0	Initial moisture content,	kg water/kg SFS
W_{eq}	Equilibrium moisture content,	kg water/kg SFS
$NaCl_0$	Initial sodium chloride content,	kg NaCl/ kg SFS
$NaCl_{eq}$	Equilibrium sodium chloride content,	kg NaCl/kg SFS
t	Time,	s
D_{NaCl}	Effective NaCl diffusivity,	m^2/s
D_W	Effective moisture diffusivity,	m^2/s
ΔD_{NaCl}	NaCl effective diffusivity increase by ultrasound	%
ΔD_W	Effective moisture diffusivity increase by ultrasound	%
L	Half length,	m
λ_n	Eigenvalues	
T_0	Initial sample thickness,	m
T	Thickness after a certain time of treatment	m
TR_0	Initial thickness ratio	
TR_{eq}	Equilibrium thickness ratio	
H_0	Initial hardness,	N
H_{eq}	Equilibrium hardness,	N
k_{TR}	Rate constant of thickness ratio,	1/s
k_H	Rate constant of hardness,	N/s
S_y	Standard deviation of the sample	
S_{yx}	Standard deviation of the estimation	

References

Andrés, A., Rodríguez-Barona, S., & Barat, J.M. (2005). Analysis of some cod-desalting process variables. *Journal of Food Engineering*, 70, 67-72.

Association of Official Analytical Chemists. Official Methods of Analysis; AOAC: Washington, DC, 1997.

Baik, O. D., & Mittal, G. S. (2003). Kinetics of tofu color changes during deep-fat frying. *LWT-Food Science and Technology*, 36, 43-48.

Barat, J. M., Gallart-Jornet, L., Andrés, A., Akse, L., Carlehög, M., & Skjerdal, O. T. (2006). Influence of cod freshness on the salting, drying and desalting stages. *Journal of Food Engineering*, 73, 9-19.

Barat, J.M., Rodríguez-Barona, S., Andrés, A. & Visquert, M. (2004). Mass transfer analysis during the cod desalting process. *Food Research International*, 37, 203-208.

Bjørkevoll, I. Olsen, J., & Olsen, R.L. (2004). Rehydration of salt-cured cod using injection and tumbling technologies. *Food Research International*, 37, 925-931.

Blasco, R., Esteve, M. J., Frígola, A., & Rodrigo, M. (2004). Ascorbic acid degradation kinetics in mushrooms in a high-temperature short-time process controlled by a thermoresistometer. *LWT-Food Science and Technology*, 37, 171-175.

Cárcel, J.A., Benedito, J., Rosselló, C., & Mulet, A. (2007a). Influence of ultrasound intensity on mass transfer in apple immersed in a sucrose solution. *Journal of Food Engineering*, 78, 472-479.

Cárcel, J. A., Benedito, J., Bon, J., & Mulet, A. (2007b). High intensity ultrasound effects on meat brining. *Meat science*, 76, 611-619.

Cárcel, J. A., García-Pérez, J. V., Benedito, J., Mulet, A., 2012. Food process innovation through new technology: Use of ultrasound. *Journal of Food Engineering*, 110, 200-207.

Chemat, F., Zill-e-Huma, & Khan, M.K. (2011). Applications of ultrasound in food technology: processing, preservation and extraction. *Ultrasonics Sonochemistry*, 18, 813–835.

Crank, J. (1975). *The Mathematics of Diffusion*. London: Oxford University Press.

Fernandes, F. A. N., Gallão, M. I., & Rodrigues, S. (2008). Effect of osmotic dehydration and ultrasound pre-treatment on cell structure: melon dehydration. *LWT-Food Science and Technology*, 41, 604-610.

Gabaldón-Leyva, C. A., Quintero-Ramos, A., Barnard, J., Balandrán-Quintana, R. R., Talamás-Abbud, R., & Jiménez-Castro, J. (2007). Effect of ultrasound on the mass transfer and physical changes in brine bell pepper at different temperature. *Journal of Food Engineering*, 81, 374-379.

Garau, M. C., Simal, S., Femenia, A., & Rosselló, C. (2006). Drying of orange skin: drying kinetics modelling and functional properties. *Journal of Food Engineering*, 75, 288-295.

Hernando, I., Llorca, E., Puig, A. & Lluch, M.A. (2011). Microstructure. In L.M.L., M.L. Leo & F. Toldra (Eds.), Handbook of Seafood and Seafood Products Analysis (pp. 139-151). Boca Raton FL: CRC Press Taylor & Francis Group.

Jayasooriya, S. D., Bhandari, B. R., Torley, P., & D'Arcy, B. R. (2004). Effect of high power ultrasound waves on properties of meat: a review. *International Journal of Food Properties*, 7, 301-319.

Kulkarni, V. M., & Rathod, V. K. (2014). Mapping of an ultrasonic bath for ultrasound assisted extraction of mangiferin from *Mangifera indica* leaves. *Ultrasonics Sonochemistry,* 21, 606-611.

Martínez-Alvarez, O., & Gómez-Guillén, C. (2013). Influence of mono- and divalent salts on water loss and properties of dry salted cod fillets. *LWT-Food Science and Technology*, 53, 387-394.

Mulet, A., 1994, Drying modelling and water diffusivity in carrots and potatoes. *Journal of Food Engineering,* 22, 329-348.

Oliveira, H. , Pedro S., Nunes, M. L., Costa, R., & Vaz-Pires, P. (2012). Processing of salted cod (*Gadus* spp.): a review. *Comprehensive Reviews in Food Science and Food Safety*, 11, 546-564.

Ozuna, C., Puig, A., García-Pérez, J.V., Mulet, A., & Cárcel, J.A. (2013). Influence of high intensity ultrasound application on mass transport, microstructure and textural properties of pork meat (*Longissimus dorsi*) brined at different NaCl concentrations. *Journal of Food Engineering*, 119, 84-93.

Pananun, T., Montalbo-Lomboy, M., Noomhorm, A., Grewell, D., & Lamsal, B. (2012). High-power ultrasonication-assisted extraction of soybean isoflavones and effect of toasting. *LWT-Food Science and Technology*, 47, 199-207.

Salvador, Â. C., Saraiva, J. A., Fidalgo, L. G., & Delgadillo, I. (2013). Effect of high pressure on cod (*Gadus morhua*) desalting. *High Pressure Research*, 33, 432-439.

Sánchez, E. S., Simal, S., Femenia, A., Benedito, J., & Rosselló, C. (1999). Influence of ultrasound on mass transport during cheese brining. *European Food Research and Technology*, 209, 215-219.

Singh, R. P. & Heldman, D.R. (2001). *Introduction to Food Engineering*. Academic Press (3rd ed.). San Diego, USA.

Siró, I., Vén, C., Balla, C., Jónás, G., Zeke, I., & Friedrich, L. (2009). Application of an ultrasonic assisted curing technique for improving the diffusion of sodium chloride in porcine meat. *Journal of Food Engineering*, 91, 353-362.

Stadnik, J., Dolatowski, Z. J., & Baranowska, H. M. (2008). Effect of ultrasound treatment on water holding properties and microstructure of beef (*m. semimembranosus*) during ageing. *LWT-Food Science and Technology*, 41, 2151-2158.

Thorarinsdottir, K. A., Arason, S., Sigurgisladottir, S., Gunnlaugsson, V. N. Johannsdottir, J., & Tornberg, E. (2011). The effects of salt-curing and salting procedures on the microstructure of cod (*Gadus morhua*) muscle. *Food Chemistry*, 126, 109-115.

Figure captions

Fig. 1 Desalting set-up. A) chiller B) valve C) heat exchanger D) pump E) cooling reservoir F) ultrasonic bath G) sample holder H) thermocouples I) cod samples J) ultrasonic transducers K) data logger L) ultrasonic generator M) Computer.

Fig. 2. Acoustic pressure (bar) distribution in the ultrasonic bath with an applied electric power of 750 W (A) and 1500 W (B) in a horizontal section at 100 mm from the water surface.

Fig. 3 Experimental NaCl (A) and moisture (B) transport kinetics of salted cod slices (thickness 5 mm) desalted with (US, 40 kHz, 750 and 1500 W) and without ultrasound application (CONTROL). Average values (each point represents the average of 12 measurements; 4 independently desalted samples analyzed in triplicate) and LSD intervals ($p<0.05$).

Fig 4. Evolution of thickness ratio vs time (A) and vs moisture content (B) during desalting of salted cod with (US, 40 kHz, 750 and 1500 W) and without ultrasound application (CONTROL). Average values (each point represents the average of 8 measurements) and LSD intervals ($p<0.05$).

Fig 5. Evolution of hardness vs time (A) and vs moisture content (B) during desalting of salted-cod with (US, 40 kHz, 750 and 1500 W) and without ultrasound application (CONTROL). Average values (each point represents the average of 30 measurements) and LSD intervals ($p<0.05$).

Fig 6. Longitudinal (A) and transversal (B) section of salted cod (*Gadus morhua*) fibers observed by SEM (x500). S: NaCl deposits, IS: Interfibrillar space.

Fig 7. Longitudinal section observed by SEM-EDX (A, B and C; x500) and LM (D, E and F; x4) of cod loin desalted for 180 min without (CONTROL, A, D), and with US at 750 (B, E) and 1500 W (C, F). IS: Interfibrillar space.

Table captions

Table 1. Average values and confidence intervals (95%) of effective diffusivity of moisture (D_W) and NaCl (D_{NaCl}) identified from modeling of cod desalting (4±1 ºC) with (US, 40 kHz, 750 and 1500 W) and without US application (CONTROL) and percentage of explained variance by the model (VAR (%)). ΔD_W and ΔD_{NaCl} (%) are the increases in effective diffusivity produced by ultrasound application.

Table 2. First-order kinetic parameters for thickness ratio (TR_{eq}, K_{TR}) and evolution of hardness (H_{eq}, K_H) during cod desalting (4±1 ºC) with (US, 40 kHz, 750 and 1500 W) and without US application (CONTROL). Average ± confidence intervals of the estimation (95%) are shown.

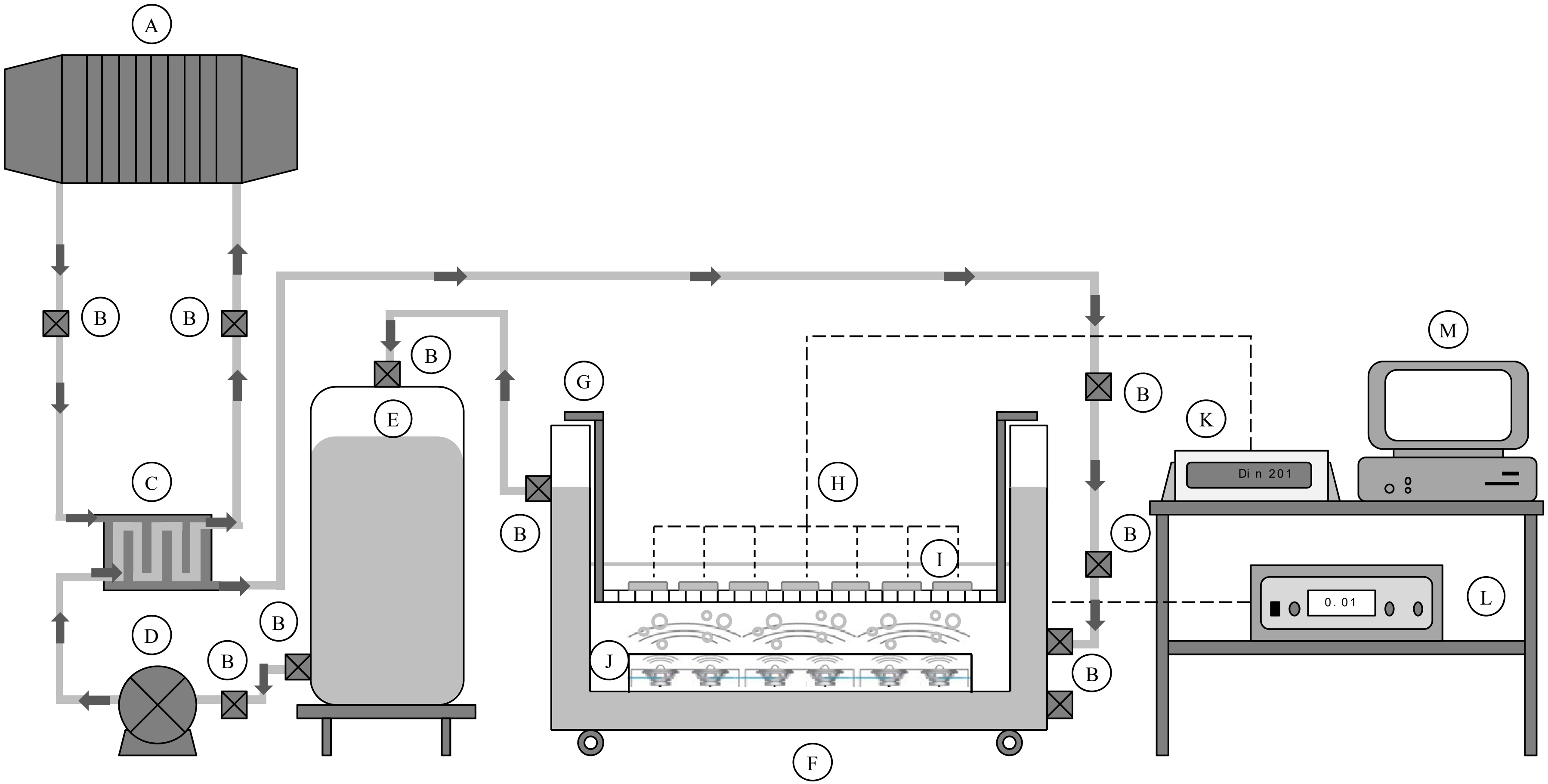

Fig 1

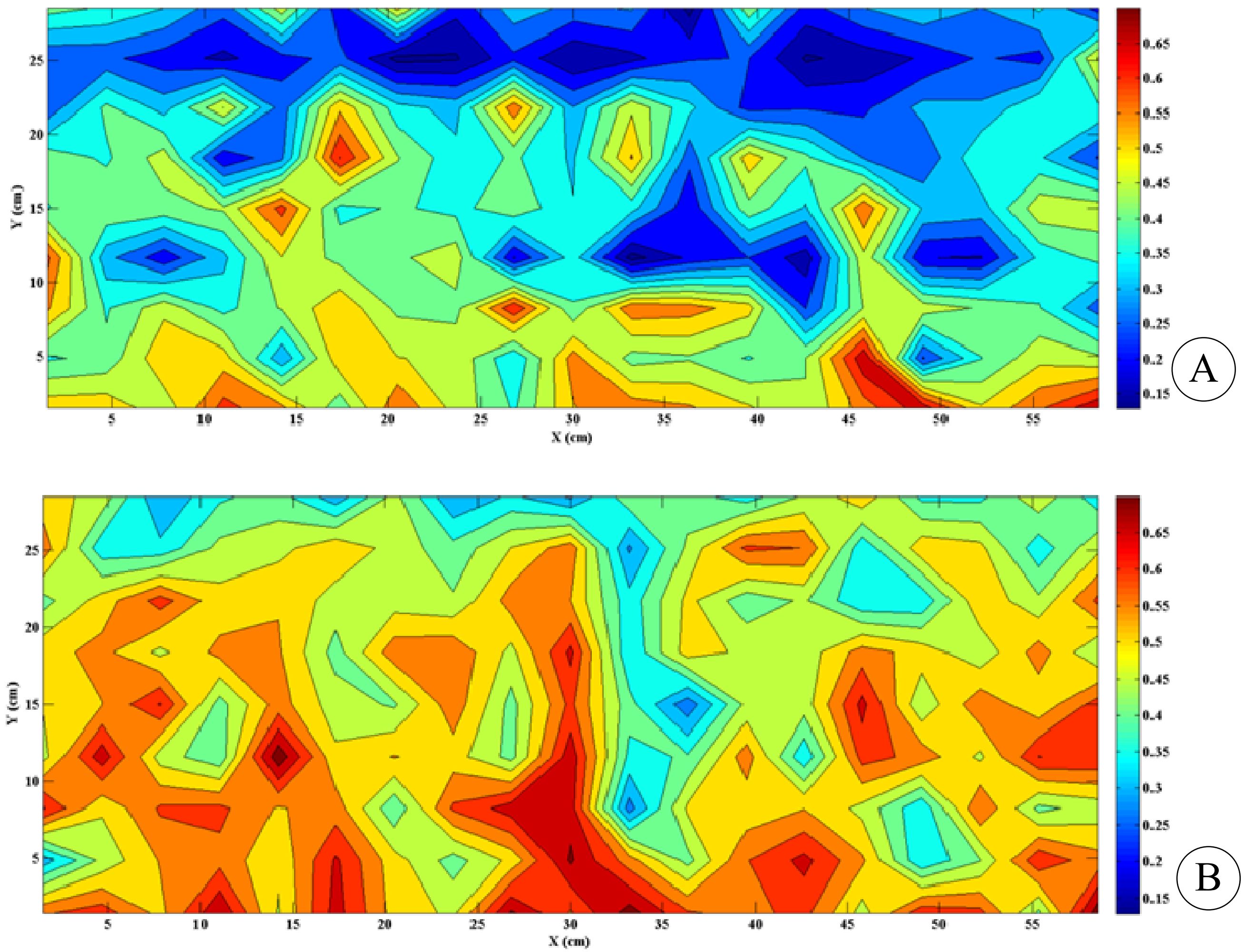
Y (cm)
X (cm)
5
10
15
20
25
30
35
40
45
50
55
0.15
0.2
0.25
0.3
0.35
0.4
0.45
0.5
0.55
0.6
0.65
A
B

Fig 2

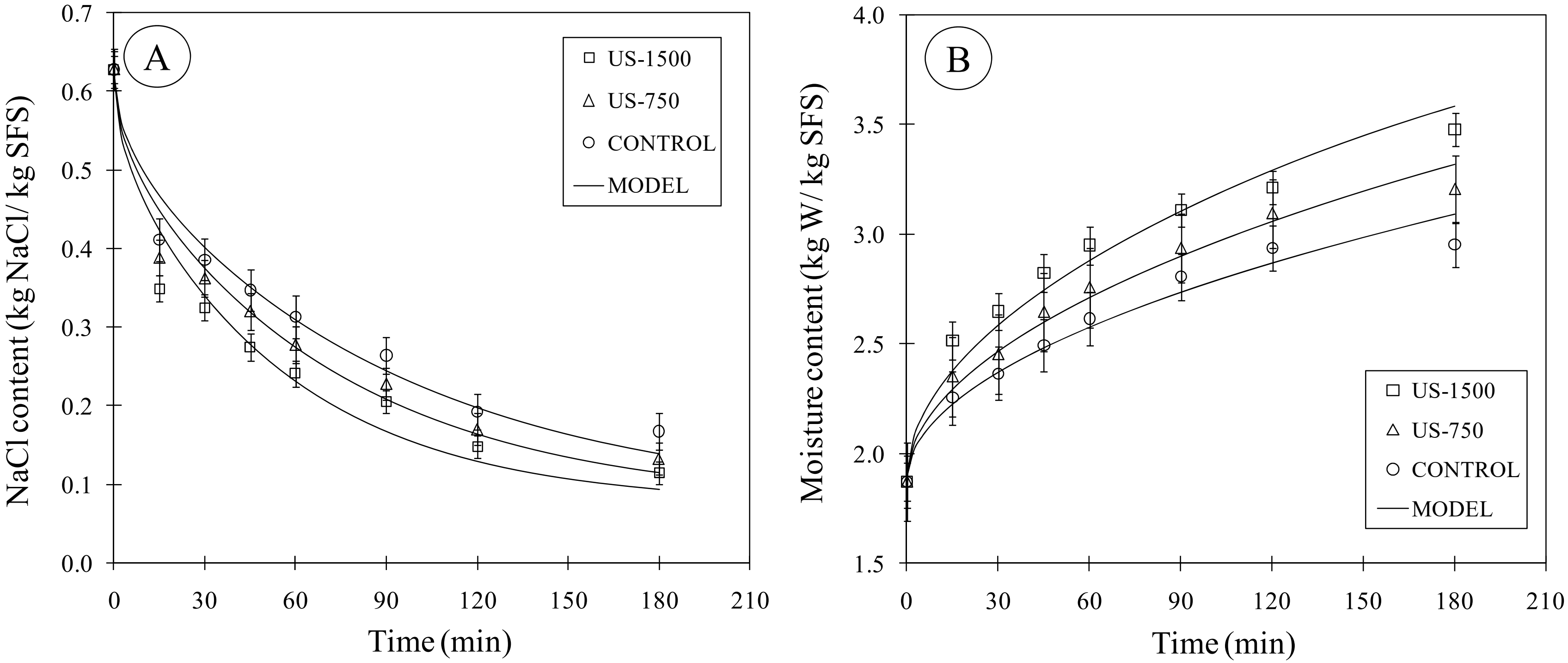
A
NaCl content (kg NaCl/ kg SFS)
0.0
0.1
0.2
0.3
0.4
0.5
0.6
0.7
Time (min)
0
30
60
90
120
150
180
210
US-1500
US-750
CONTROL
MODEL
B
Moisture content (kg W/ kg SFS)
1.5
2.0
2.5
3.0
3.5
4.0
Time (min)
0
30
60
90
120
150
180
210
US-1500
US-750
CONTROL
MODEL

Fig 3

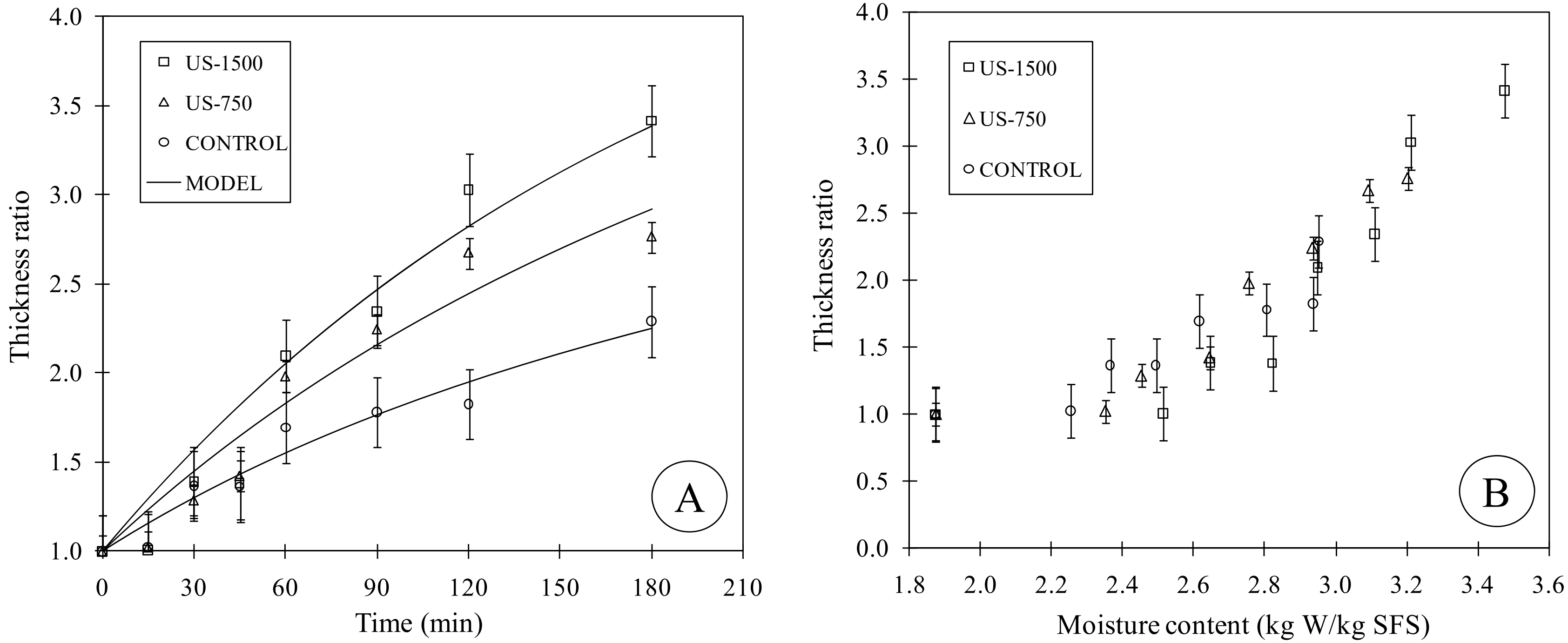
US-1500
US-750
CONTROL
MODEL
A
Thickness ratio
Time (min)
4.0
3.5
3.0
2.5
2.0
1.5
1.0
0
30
60
90
120
150
180
210
US-1500
US-750
CONTROL
B
Thickness ratio
Moisture content (kg W/kg SFS)
4.0
3.5
3.0
2.5
2.0
1.5
1.0
0.5
0.0
1.8
2.0
2.2
2.4
2.6
2.8
3.0
3.2
3.4
3.6

Fig 4

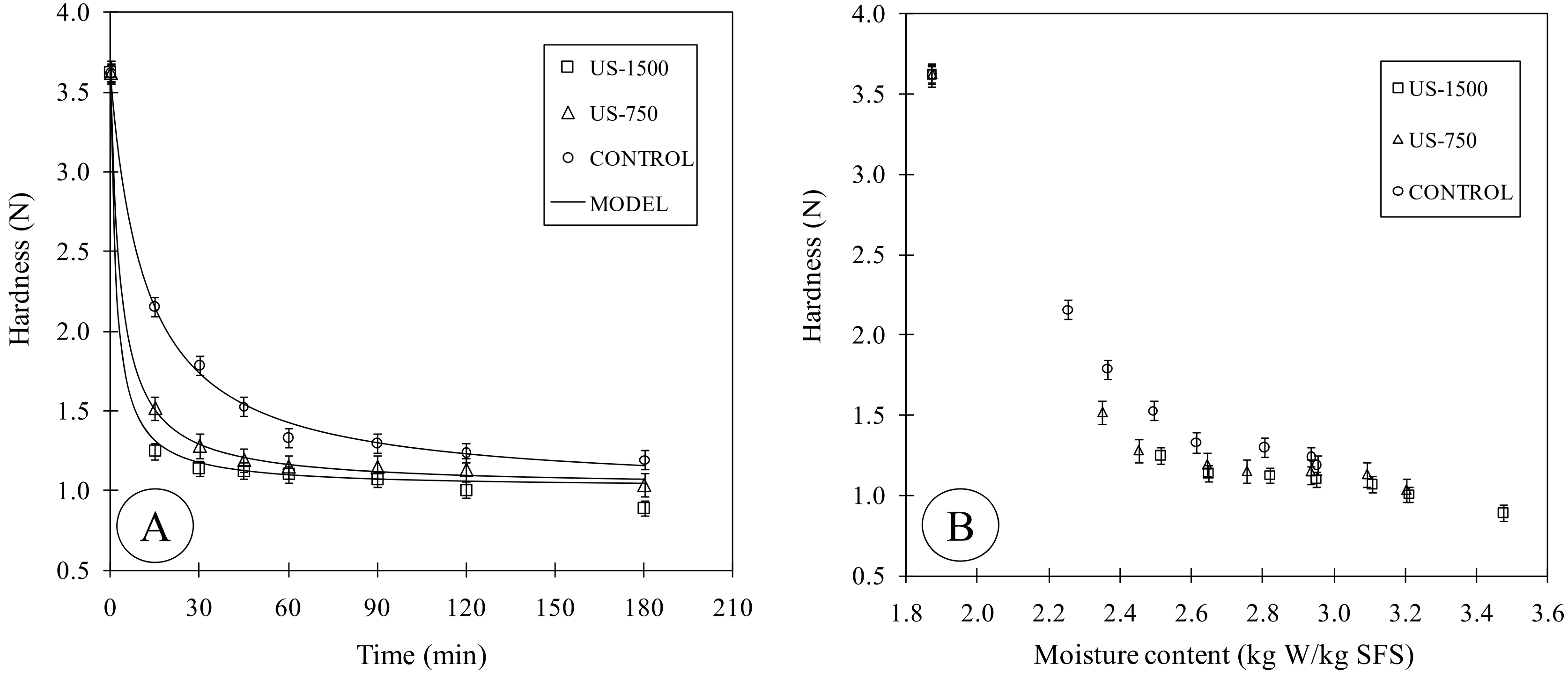
A
Hardness (N)
Time (min)
US-1500
US-750
CONTROL
MODEL
B
Hardness (N)
Moisture content (kg W/kg SFS)
US-1500
US-750
CONTROL

Fig 5

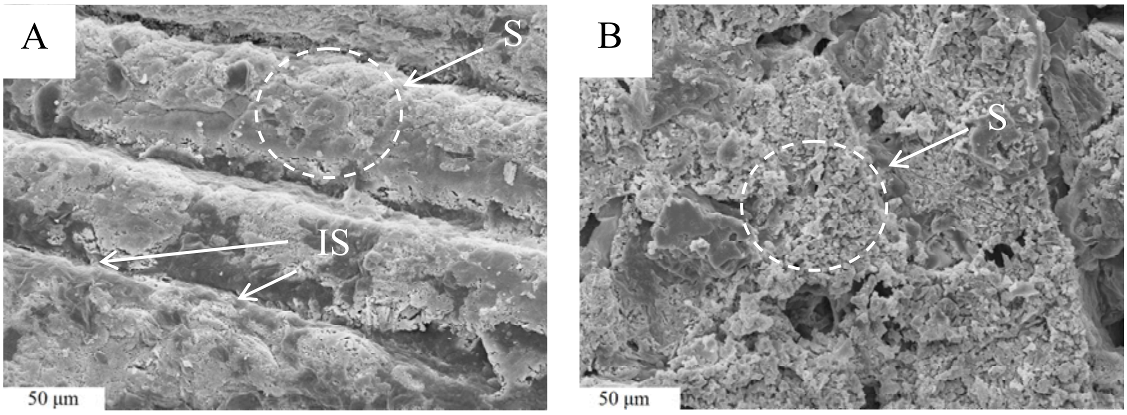

Fig 6

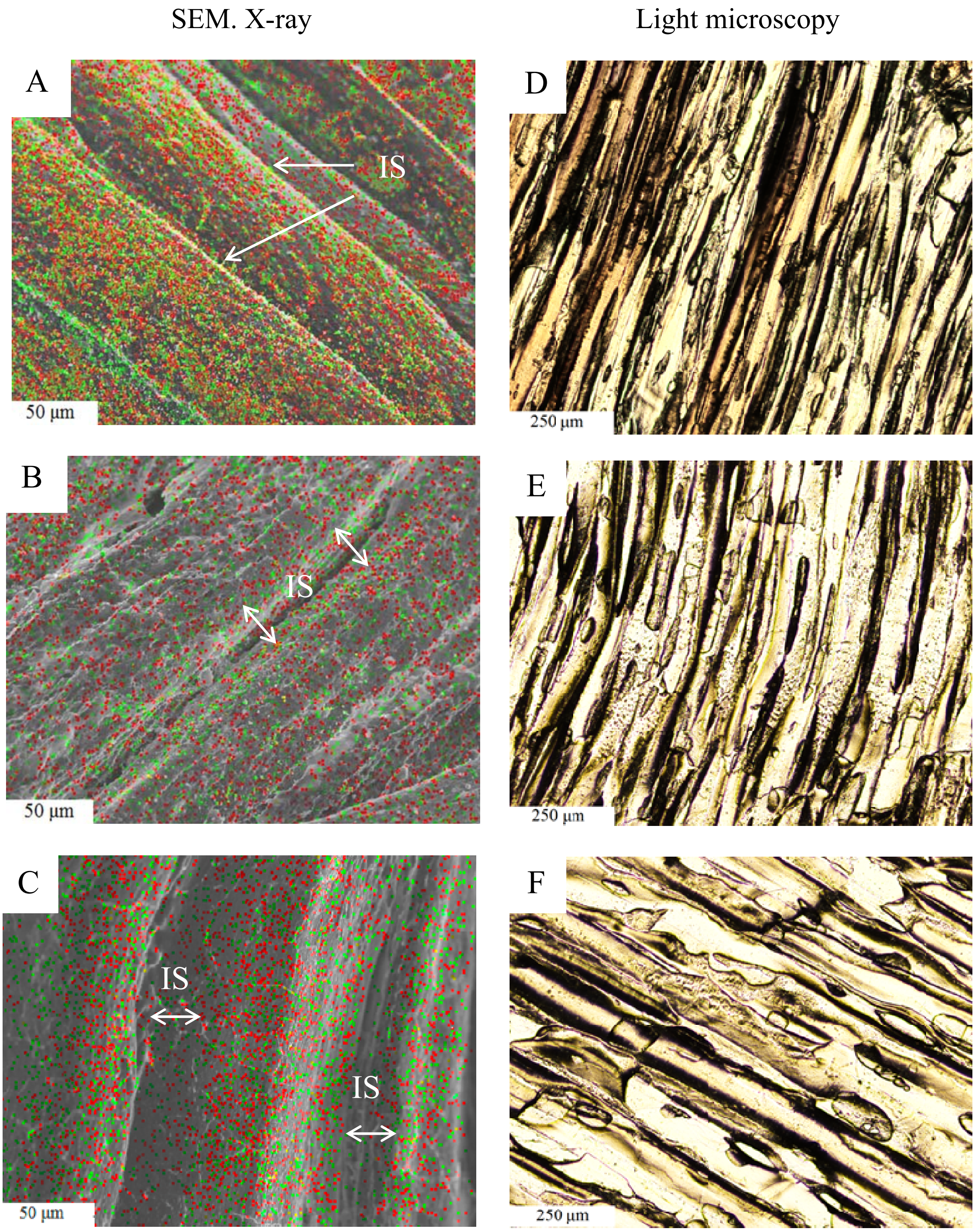
SEM. X-ray
Light microscopy
A
IS
50 µm
D
250 µm
B
IS
50 µm
E
250 µm
C
IS
IS
50 µm
F
250 µm

Fig. 7

Table 1

	NaCl transport			Water transport		
	D_{NaCl} (10^{-10}) [m^2/s]	ΔD_{NaCl} (%)	VAR (%)	D_W (10^{-10}) [m^2/s]	ΔD_W (%)	VAR (%)
CONTROL	4.6 ± 0.8	-	95.0	1.1 ± 0.2	-	95.0
US-750	5 ± 1	24.9	95.7	1.5 ± 0.2	41.3	97.2
US-1500	7.0 ± 1.1	61.9	93.3	2.2 ± 0.3	102.8	95.0

	Swelling evolution			Hardness evolution		
	TR_{eq}	k_{TR} (10^{-3}) [min^{-1}]	VAR (%)	H_{eq} (N)	k_H [min^{-1}]	VAR (%)
CONTROL	3.1±0.2	5.1±2.1	94.4	1.26±0.08	0.06±0.02	99.1
US-750	4.1±0.4	5.2±1.0	92.9	1.14±0.06	0.12±0.03	99.6
US-1500	4.9±0.4	5±1	92.7	1.15±0.09	0.17±0.07	99.2